

Supplementary Material

Description of the computational methods

We used the Quantum-Espresso¹ suite of programs with unrestricted density functional theory², PBE³ exchange-correlation functional and a plane-wave basis set. Ultra-soft pseudopotentials were employed with a 30 Ryd kinetic energy cut-off for the smooth part of the wavefunctions and 180 Ryd for the augmented charge density. The molecules were placed in a cubic periodic cell of linear dimension 25 atomic units. The dynamical matrix was constructed by the frozen-phonon method. The IR cross-section was calculated by evaluating the Born effective charges and projecting them onto the normal modes to obtain the transition dipole⁴. Rigid linear and rotational modes of motion were projected out by standard methods⁵, and the acoustic sum-rule⁶ was imposed on the matrix elements of the Born charge tensors. We emphasize that we do not employ any ad hoc, a posteriori corrections to the frequencies or intensities to improve the predicted IR frequencies. Our methods have been validated extensively⁷ by studying synthetic models of Fe₂H₂ase of known high-resolution (crystal) structure. We have shown that well-converged calculations of energy, structure and vibrations accurately reproduce the IR spectra of these model systems. It is now well established that fully converged density functional computations generate accurate IR spectra^{7, 8}. Qualitative discrepancies between theory and experiment most probably arise from inadequate structural models. Consequently, we were able to distinguish among the various structural isomers that differ in their CO/CN arrangement, an issue of direct relevance for this paper.

We have also employed the “string” method⁹ for calculating the reaction path leading from model 4 to model 3.

Enhanced coupling between the CO ligands on the distal Fe in Model 1 compared with model 2

A vibrational distortion of one CO will perturb all the MO's that couple the two groups and thus form a charge perturbation on the other CO. The more such MO's couple the two groups, the larger the charge perturbation and thus the vibrational coupling. We can quantify this coupling by projecting each MO onto a linear combination of (pseudo-)atomic orbitals (atomic orbitals consistent with the pseudo-potential used here⁷). We then calculate the triple product of the square of the amplitude on the Fe atom, the sum of the squares of the amplitudes on each atom in one CO group, and the corresponding sum for the other CO. Finally, we sum over all MO's in the relevant energy range, -10 to -6 eV. The result is 30% larger in 1 than in 2, a clear indication of stronger coupling in 1.

The effect of replacing the PDT by a DTN bridge

The isotope shifts in the infrared spectra of the CO-inhibited form of [Fe-Fe]-hydrogenase can only be explained by the specific arrangement of the CO/CN ligands around the distal Fe. This result does not depend on the nature of the bridging ligand. Indeed, replacing the bridging PDT by a DTN in model 2 gives the spectra shown in Figure S1 below. It is evident from this figure that the spacing between the modes and their intensities differ significantly from experiment, especially for the terminal CO modes. More importantly, the isotope shifts are incorrect; only one mode shows a substantial shift. This is quite similar to the result in Figure 2 **Error! Reference source not found.**(a) of the paper. We also checked that including nearby protein groups, such as cubane Fe₄S₄, does not change our main qualitative conclusion on the arrangement of the CO/CN ligands.

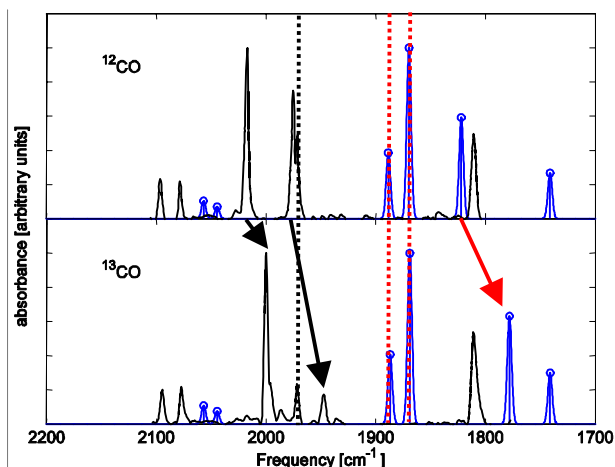


Figure S1 Experimental spectra (black line, reproduced with permission from Ref.¹⁰) and simulated spectra of Fe₂H₂ase-CO model 2 having a DTN bridge (blue line). A Gaussian broadening of 2 cm⁻¹ is used. Dashed lines mark the terminal CO modes unchanged by labeling, and the arrows show the modes that shift consequent to labeling of the exogenous CO with ¹³C.

Spin density distributions

Figure S2 below shows the spin density distribution for models 1, 2 and 4. The main quasi-symmetry plane is formed by the two Fe atoms and the central carbon atom of the PDT bridging ligand. Though strictly speaking this is not a symmetry plane with respect to the ligands around the *proximal* Fe, these figures demonstrate that the spin density around this atom is quite symmetric in models 1 and 2. The distribution around the *distal* Fe is also symmetric in model 1 but clearly asymmetric in model 2. Similar asymmetry exists also in the active-ready state, model 4. An asymmetric spin distribution gives rise to a rhombic EPR g-tensor, as observed experimentally for the active-ready state in CpI¹¹ and DdHase¹². Our results suggest that only model 1, having a quasi-reflection plane, can explain the observed change from a rhombic to an axial EPR g-tensor upon inactivation with CO. In that case the z principal axis of the g-tensor lies in the symmetry plane with symmetrically equivalent x,y axes 45° to the symmetry plane. These figures also illustrate the spin redistribution upon inactivation, from a localized spin density on the distal Fe to an even distribution over the two Fe atoms. This spin localization on the distal Fe strongly suggests the availability of an electron for charge transfer to an incoming proton in the active-ready state.

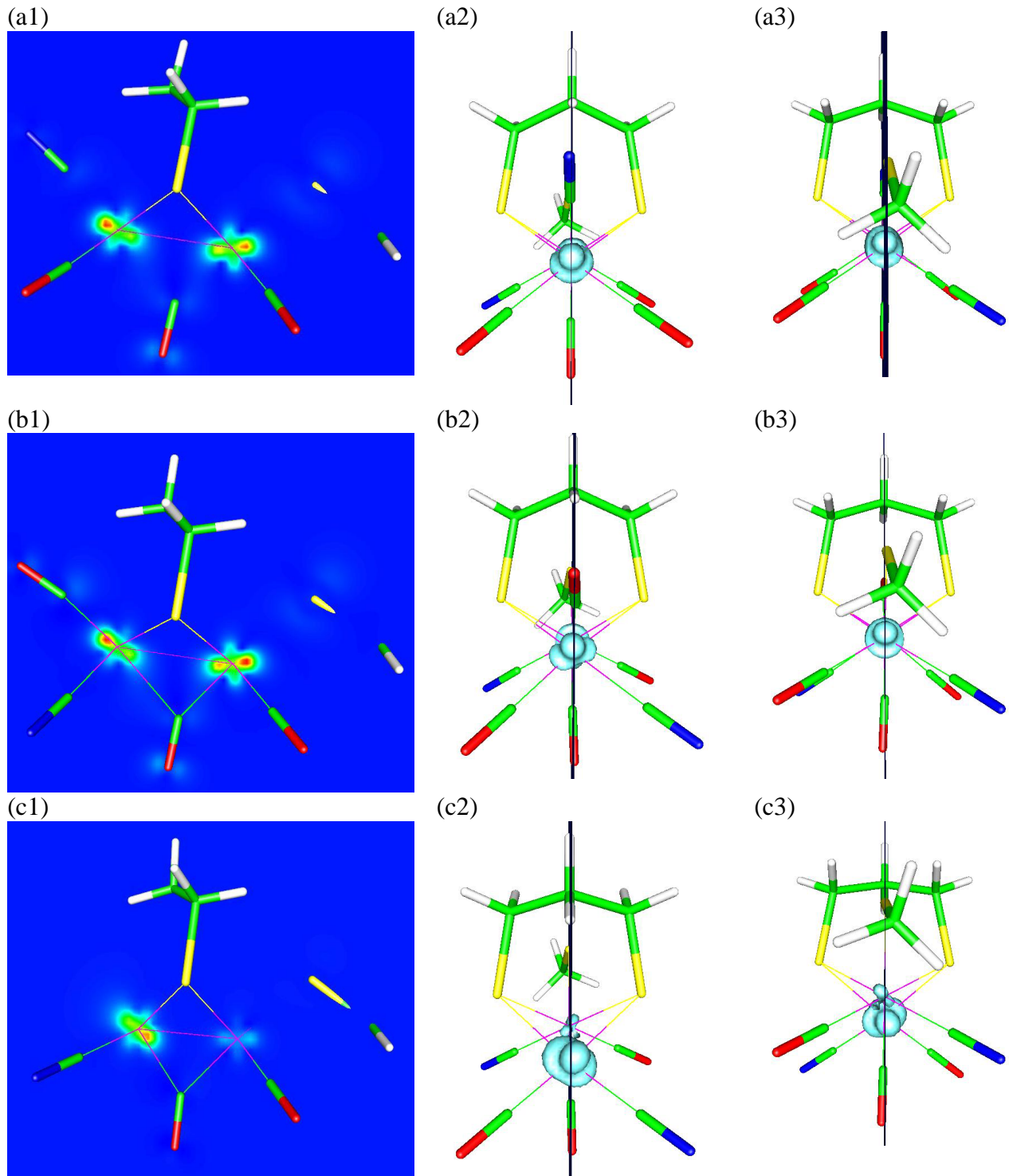


Figure S2 Visualization via gOpenMol¹³ of the spin-density distributions for models 1 (a1-a3), model 2 (b1-b3) and model 4 (c1-c3). Subfigures a1, b1 and c1 show a side view with the spin density on a cut-plane formed by the two Fe nuclei and the central C nucleus of the PDT bridge. The color scale goes from red for high spin-density to blue for zero density. Subfigures a2, b2 and c2 are oriented toward the distal Fe, showing an iso-density surface. The black line bisecting these figures is the cut-plane presented above. Subfigures a3, b3 and c3 are similar to a2-c2 but are oriented towards the proximal Fe.

1. *Quantum-ESPRESSO*, 3.0; 2005 (www.quantum-espresso.org).
2. Parr, R. G.; Yang, W., *Density-Functional Theory of Atoms and Molecules*. Oxford University Press: 1989; Vol. 16.
3. Perdew, J. P.; Burke, K.; Ernzerhof, M., *Phys. Rev. Lett.* **1997**, 78, (7), 1396-1396; Perdew, J. P.; Burke, K.; Ernzerhof, M., *Phys. Rev. Lett.* **1996**, 77, (18), 3865-3868.
4. Gonze, X.; Lee, C., *Phys. Rev. B* **1997**, 55, (16), 10355-10368.
5. Wilson, E. B., *Molecular vibrations: The theory of infrared and Raman vibrational spectra*. McGraw-Hill: 1955.
6. Pick, R. M.; Cohen, M. H.; Martin, R. M., *Phys. Rev. B* **1970**, 1, (2), 910-919.
7. Zilberman, S.; Stiefel, E. I.; Cohen, M. H.; Car, R., *J. Phys. Chem. B* **2006**, 110, 7049-7057.
8. Baroni, S.; de Gironcoli, S.; Dal Corso, A.; Giannozzi, P., *Rev. Mod. Phys.* **2001**, 73, 515-562.
9. Kanai, Y.; Tilocca, A.; Selloni, A.; Car, R., *J. Chem. Phys.* **2004**, 121, (8), 3359-3367.
10. Chen, Z. J.; Lemon, B. J.; Huang, S.; Swartz, D. J.; Peters, J. W.; Bagley, K. A., *Biochemistry* **2002**, 41, (6), 2036-2043.
11. Patil, D. S.; Huynh, B. H.; He, S. H.; Peck, H. D.; Dervartanian, D. V.; Legall, J., *J. Am. Chem. Soc.* **1988**, 110, (25), 8533-8534; Patil, D. S.; He, S. H.; Dervartanian, D. V.; Legall, J.; Huynh, B. H.; Peck, H. D., *FEBS Lett.* **1988**, 228, (1), 85-88; Bennett, B.; Lemon, B. J.; Peters, J. W., *Biochemistry* **2000**, 39, (25), 7455-7460.
12. Adams, M. W. W., *J. Biol. Chem.* **1987**, 262, (31), 15054-15061.
13. Laaksonen, L. *gOpenMol*, 3.0; (<http://www.csc.fi/gopenmol>).